ACS OMEGA

Open Access

http://pubs.acs.org/journal/acsodf

Article

Exploring KRas Protein Dynamics: An Integrated Molecular Dynamics Analysis of KRas Wild and Mutant Variants

Showkat Ahmad Mir, Binata Nayak,* Nada H Aljarba, Vinoth Kumarasamy,* Vetriselvan Subramaniyan, and Bikram Dhara*

Cite This: *ACS Omega* 2024, 9, 30665−30674

Read Online

ACCESS | Metrics & More | Article Recommendations

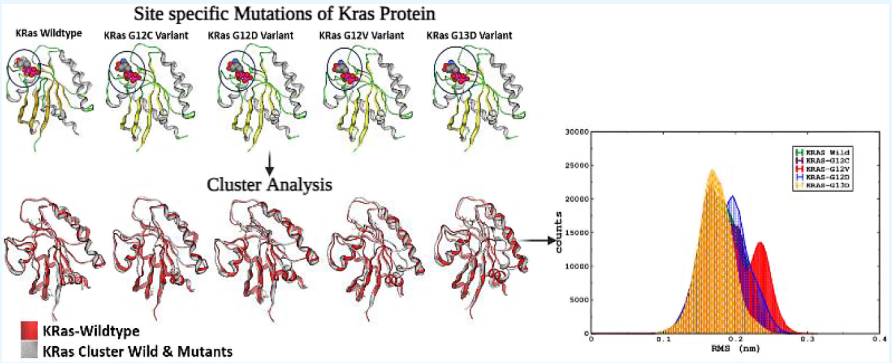

ABSTRACT: This study employs a comprehensive approach combining protein retrieval, sequence alignment, and molecular dynamics simulations to investigate the structural dynamics and stability of wild-type KRas and its mutated variants (G12C, G12D, G12V, and G13D). The selected protein structures were retrieved from the Protein Data Bank (PDB) and prepared by using visual molecular dynamics (VMD) software. Sequence alignment using Clustal Omega provided a detailed comparison of the amino acid sequences, focusing on key mutation sites. Molecular dynamics simulations, performed with Gromacs, revealed distinct conformational changes and stability patterns in the wild-type and mutated KRas proteins over 100 ns. Clustering analysis identified higher conformational changes in the second α-helix of the mutated variants. The root-mean-square deviation (RMSD) distribution analysis showed variant-specific conformational dynamics, with G12V and G12D exhibiting slightly higher average RMSD values. Furthermore, clustering and RMSD analyses of specific amino acid residues (12, 13, 51, and 118) highlighted their roles in maintaining overall stability and influencing structural dynamics. The results indicate that mutations at positions 12 and 13 disrupt normal cycling between wild and mutated variants, leading to the persistent activation of KRas. Additionally, principal component analysis (PCA) elucidated unique conformational dynamics in mutated variants. Free energy landscape (FEL) analysis revealed alterations in the thermodynamic stability of mutated variants compared with the wild type. Overall, this study provides a detailed understanding of the structural changes associated with oncogenic mutations in KRas, offering insights crucial for targeted therapeutic strategies in KRas-driven cancers.

INTRODUCTION

The KRas gene (Ki-ras2 Kirsten rat sarcoma viral oncogene homologue), a key member of the RAS family, is a critical player in orchestrating cellular signaling pathways, and its encoded product, the KRAS protein, serves as a small GTPase transductor. This protein is central to the regulation of cell division and acts as a vital intermediary in transmitting external signals to the cell nucleus. The intricate signaling network in which KRas participates plays a fundamental role in determining cellular responses to growth factors and environmental cues. The proper functioning of KRAS is essential for maintaining normal cell growth and differentiation. However, the aberrant functioning of the KRas gene is frequently implicated in various human cancers, making it a prominent focus of oncological research.[1] In normal cells, KRas is tightly regulated by various signaling cascades. Mutations in the KRas gene disrupt these regulatory mechanisms, leading to dysregulated cell signaling. This disruption ultimately results in uncontrolled cell proliferation—a hallmark of tumorigenesis and a key contributor to cancer development.[2] Of particular

Received: March 27, 2024
Revised: May 14, 2024
Accepted: June 3, 2024
Published: July 1, 2024

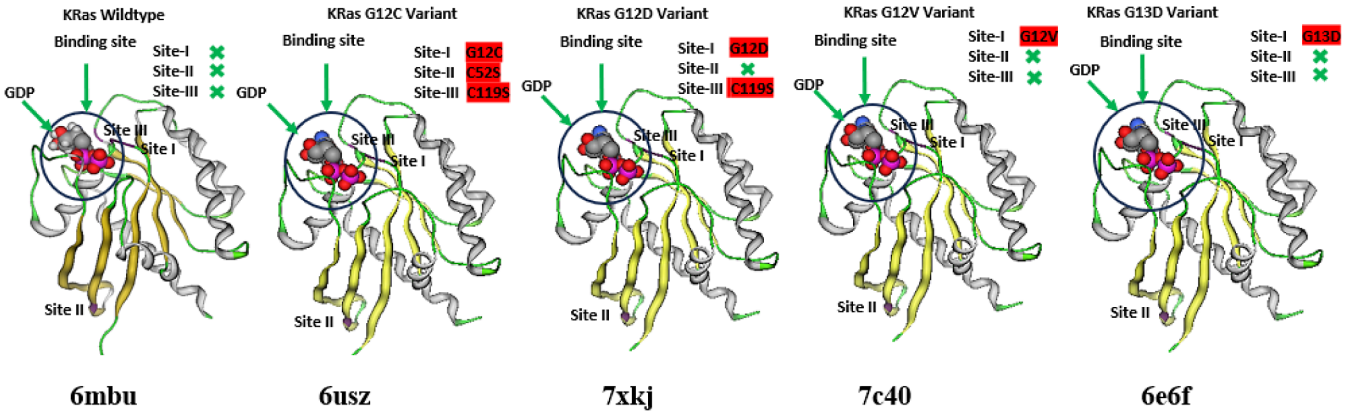

Figure 1. X-ray crystallographic structures of the wild and mutated variants of the KRas protein. The marrow colors represented as sites-I, II, and III are the prone sites of mutations; also, the cross mark in green color represents no mutations, respectively.

interest in the context of oncogenic transformation are mutations occurring at codons 12 and 13 of the KRas gene. The substitutions of glycine at position 12 with cysteine (G12C), valine (G12V), or aspartate (G12D), as well as the substitution of glycine at position 13 with aspartate (G13D), are prevalent mutations associated with a heightened risk of cancer.[3,4] These mutations induce a state of constitutive activation in the KRas protein, disrupting its normal regulatory functions. This persistent activation leads to sustained signaling and uncontrolled cell growth and division, all of which contribute significantly to the development and progression of cancer.[5] To unravel the molecular mechanisms underlying the oncogenic potential of these mutations, a comprehensive understanding of the structural dynamics and stability changes induced by them becomes paramount. In this study, we employ molecular dynamics simulations—a sophisticated computational technique—to explore the conformational landscape of both the wildtype and mutated KRas proteins. By simulating the motions and interactions of individual atoms over time, we gain nuanced insights into the dynamic behavior of these proteins at the atomic level. The primary focus of the investigation is on the KRas wildtype and four mutated variants—G12C, G12V, G12D, and G13D.[6,7] The molecular dynamics simulations generate trajectories that capture the dynamic behavior of these proteins, allowing for a detailed analysis of conformational changes and stability profiles. The GDP- and GTP-bound KRas insights from multiple replica Gaussian accelerated molecular dynamics and free energy analysis and mutation probabilities of KRAS G12 missense mutants and their long-time scale dynamics by atomistic molecular simulations and Markov state modeling were explored by Pantsar et al., 2018[28] and Mukerjee et al., 2021.[29] The more persistent KRas mutations remain unexplored. The findings from this research are anticipated to provide valuable information that can be leveraged in the development of targeted therapeutic strategies against cancers driven by KRas mutations. Ultimately, this work contributes to advancing our understanding of the structural biology of KRas, paving the way for the design of more effective and targeted treatments for KRas-driven malignancies.

MATERIAL AND METHODS

Protein Retrieval. The protein structures utilized in this study included mutated variants of KRAS at codons 12 and 13, the wildtype KRas structure (PDB ID: 6mbu)[7] namely G12C (PDB ID: 6USZ),[8] G12D (PDB ID: 7xkj),[6] G12V (PDB ID: 7c40),[9] and G13D (PDB ID: 6e6f),[10] sourced from the Protein Data Bank (PDB) (Berman et al., 2000) for comparative analysis. These structures were chosen based on their relevance to oncogenic transformation and their availability in the PDB (Figure 1). The structures were prepared by using visual molecular dynamics (VMD) software.[11]

Sequence Alignment Using Clustal Omega. The EMI Tools platform[12,13] is a web-based environment for bioinformatics analysis, including sequence alignment. The Clustal Omega tool was selected for the sequence alignment tool for aligning the KRAS wild-type and mutated variants. Clustal Omega[14] is a widely used program for multiple sequence alignment and is suitable for accurately aligning homologous sequences. The amino acid sequences for the KRAS wildtype and mutated variants (G12V, G12D, G12C, G13D) were retrieved from www.rcbs.org/.[15] The KRAS wildtype and mutated variant sequences were uploaded onto the EMI Tools platform. The visual representations of the sequence alignment were generated. The visualization features create figures illustrating the aligned sequences, highlighting conserved regions and identifying specific amino acid variations. The results were obtained from the sequence alignment, paying specific attention to regions where mutations occur (G12V, G12D, G12C, G13D).

Molecular Dynamics Simulations. Molecular dynamics simulations were performed using established protocols[16,17] to investigate the conformational dynamics and stability of the KRAS proteins. The Gromacs 22.4v software was employed for the preparation and execution of the simulations.[30] Following preparation of the protein structures, the hydrogen atoms were added, missing side chains were modeled, and water molecules and heteroatoms were removed. The protonation states of histidine residues ensure the correct representation of their chemical environment. Specifically, we treated the protonation states of histidine residues as follows: residue His27 was protonated at the epsilon nitrogen atom (HISE). Residue His94 was protonated at the delta nitrogen (HISD). Residue His95 was protonated at the epsilon nitrogen (HISE). Residue His166 was protonated at the epsilon nitrogen (HISE). The proteins were then solvated by 9084 sols in a periodic water box, with counterions of 7 Na^+ added for electroneutrality. The ff14SB force field was used for the parametrization of the proteins, respectively.[18] Energy minimization was performed to

https://doi.org/10.1021/acsomega.4c02671
ACS Omega 2024, 9, 30665−30674

```
pdb|6USZ|A      GMTEYKLVVVGAGGVGKSALTIQLIQNHFVDEYDPTIEDSYRKQVVIDGETCLLDILDTA   60
pdb|7C40|A      -MTEYKLVVVGAVGVGKSALTIQLIQNHFVDEYDPTIEDSYRKQVVIDGETCLLDILDTA   59
pdb|7XKJ|A      -MTEYKLVVVGADGVGKSALTIQLIQNHFVDEYDPTIEDSYRKQVVIDGETCLLDILDTA   59
pdb|6MBU|A      GMTEYKLVVVGAGGVGKSALTIQLIQNHFVDEYDPTIEDSYRKQVVIDGETCLLDILDTA   60
pdb|6E6F|A      -MTEYKLVVVGAGDVGKSALTIQLIQNHFVDEYDPTIEDSYRKQVVIDGETCLLDILDTA   59
                 ********** ************************************ ********

pdb|6USZ|A      GQEEYSAMRDQYMRTGEGFLLVFAINNTKSFEDIHHYREQIKRVKDSEDVPMVLVGNKSD   120
pdb|7C40|A      GQEEYSAMRDQYMRTGEGFLCVFAINNTKSFEDIHHYREQIKRVKDSEDVPMVLVGNKCD   119
pdb|7XKJ|A      GQEEYSAMRDQYMRTGEGFLCVFAINNTKSFEDIHHYREQIKRVKDSEDVPMVLVGNKSD   119
pdb|6MBU|A      GQEEYSAMRDQYMRTGEGFLCVFAINNTKSFEDIHHYREQIKRVKDSEDVPMVLVGNKCD   120
pdb|6E6F|A      GQEEYSAMRDQYMRTGEGFLCVFAINNTKSFEDIHHYREQIKRVKDSEDVPMVLVGNKCD   119
                 ****************** ************************************ *

pdb|6USZ|A      LPSRTVDTKQAQDLARSYGIPFIETSAKTRQGVDDAFYTLVREIRKHKEK----- 170
pdb|7C40|A      LPSRTVDTKQAQDLARSYGIPFIETSAKTRQGVDDAFYTLVREIRKHKEHHHHHH 174
pdb|7XKJ|A      LPSRTVDTKQAQDLARSYGIPFIETSAKTRQGVDDAFYTLVREIRKHKEK----- 169
pdb|6MBU|A      LPSRTVDTKQAQDLARSYGIPFIETSAKTRQGVDDAFYTLVREIRKHKEK----- 170
pdb|6E6F|A      LPSRTVDTKQAQDLARSYGIPFIETSAKTRQGVDDAFYTLVREIRKH-------- 166
                 ********************************************
```

Figure 2. Sequence alignment of KRas wildtype and mutated variants using Clustal Omega.

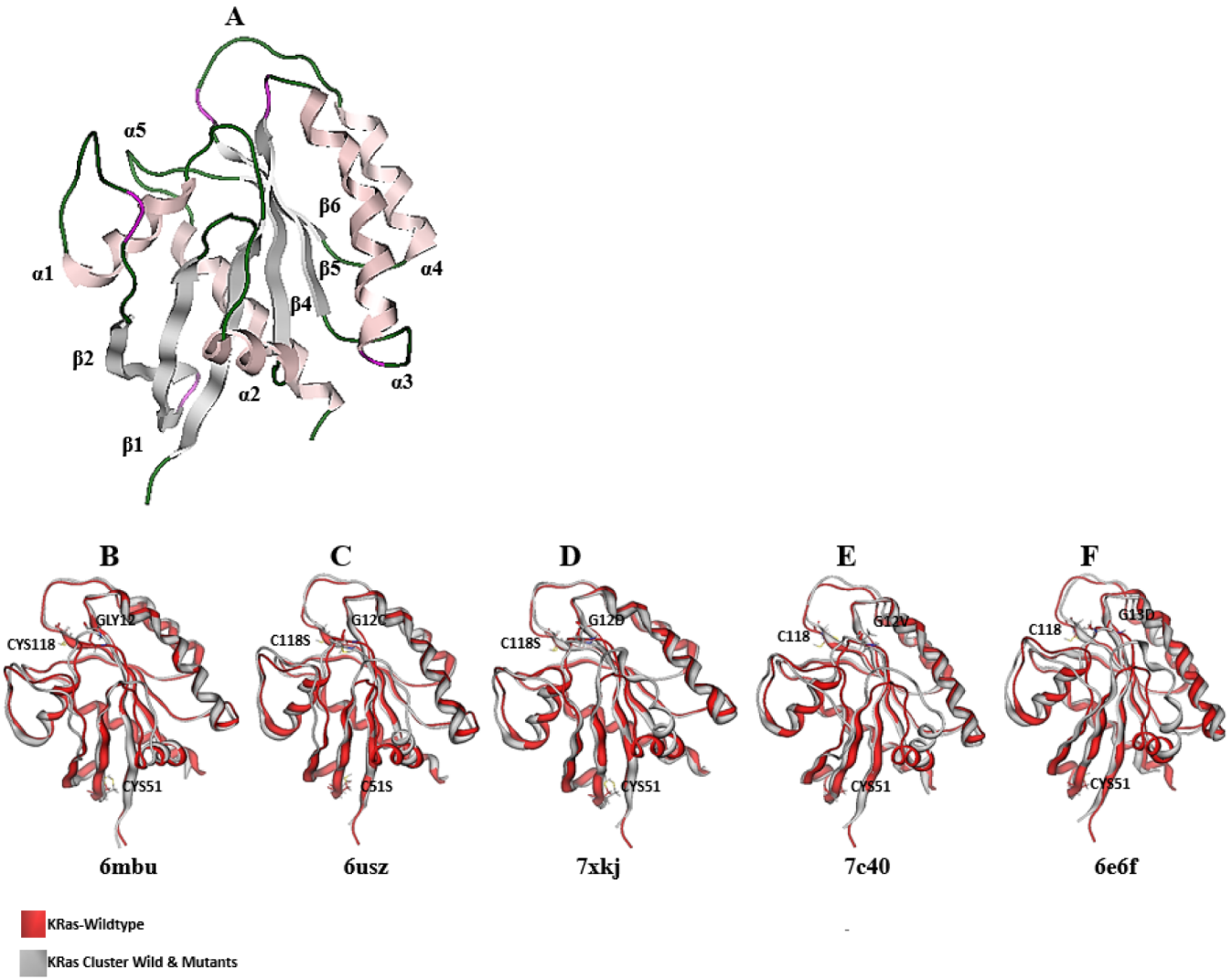

Figure 3. Cartoon and ribbon-shaped structure of KRas are illustrated in A−F. The clustering analysis of KRas wildtype and mutants was done by using the gmx cluster analysis tool and higher conformational changes were identified in the 2nd α-helix in mutated variants of KRas.

alleviate steric clashes and correct for any structural irregularities. Subsequently, the system underwent a series of equilibration steps, including gradual heating and density equilibration, to reach a stable starting point for production simulations.[19] The production molecular dynamics simulations were conducted under constant temperature (300 K) and pressure (1 atm) conditions.[20] The Langevin thermostat and the Berendsen barostat were employed to regulate temperature and pressure, respectively.[21] The MDS was performed for 100 ns with a time interval of 2 fs.[22] The resulting trajectories from

https://doi.org/10.1021/acsomega.4c02671
ACS Omega 2024, 9, 30665−30674

the simulations were analyzed by using a combination of Gromacs tools. The key structural parameters, such as root-mean-square deviation (RMSD) and root-mean-square fluctuation (RMSF), were monitored over the simulation time to assess conformational changes and stability.[23] The statistical analyses were performed using appropriate tools to extract meaningful information from the molecular dynamics trajectories. The comprehensive investigation into the structural dynamics of wild-type and mutated KRAS proteins provides insights into the conformational changes and stability associated with oncogenic mutations. The detailed analysis of the molecular dynamics simulations contributes to a deeper understanding of the molecular mechanisms underlying KRAS-driven cancers, aiding in the design of targeted therapeutic strategies.

RESULTS AND DISCUSSIONS

Sequence Alignment KRas Wildtype and Mutated Variants. The mutations in the KRas protein are more comprehensively detailed and are depicted in Figure 2. The wild-type KRAS protein is the normal, nonmutated form. Under normal conditions, KRAS acts as a molecular switch, cycling between inactive (GDP-bound) and active (GTP-bound) states, regulating downstream signaling pathways involved in cell growth and division.[24] Also, in the G12V KRas protein, the substitution of glycine with valine leads to altered conformation and enhanced affinity for GTP, favoring the active state.[25] The substitution at positions 52 and 119 introduces cysteine residues, potentially influencing the protein's interactions and stability. In G12D mutation, the mutation of glycine with aspartic acid at position 12 enhances the protein's affinity for GTP, promoting constitutive activation.[26] Cysteine substitutions at positions 52 and 119 may affect the protein's structure and interactions. The G12C mutation leads to constitutive activation by promoting GTP binding. The cysteine substitutions at positions 52 and 119 may alter the protein's structure and interactions. Besides the G12D mutation, there is an additional substitution at position 13 where glycine is replaced by aspartic acid. These mutations collectively contribute to the sustained activation of KRas. The mutations at positions 12 and 13 are strategically placed within the GTP-binding domain of KRas. This domain is crucial for the protein's ability to bind and hydrolyze GTP, serving as a molecular switch. Mutations at these positions disrupt the normal cycling between the active and inactive states, leading to a persistent active state. The substitutions at positions 52 and 119, involving the replacement of serine with cysteine, may introduce reactive thiol groups, potentially affecting protein−protein interactions and stability. Understanding these structural changes is vital for the design of targeted therapies. Scientists all over the world aim to develop drugs that specifically inhibit the aberrant, constitutively active forms of KRas, providing potential treatments for cancers driven by KRas mutations. The Protein Data Bank entries (PDB IDs) serve as valuable resources for studying the three-dimensional structures of these mutated KRas proteins, aiding in the design and optimization of targeted therapies.

Molecular Dynamics Simulations. *Clustering Analysis of Wildtype and KRas Mutants.* The RMS distribution is a measure used in molecular dynamics simulations to analyze the stability and fluctuations of protein structures over time. It calculates the root-mean-square deviation (RMSD) of the atomic positions from their average positions. The RMSD is computed by comparing the positions of atoms in each frame of the trajectory to those in a reference structure. The RMSD values indicate how much the protein structure deviates from the reference structure at each time point during the simulation. A low RMSD value signifies a stable structure, indicating that the protein maintains its overall conformation. On the other hand, higher RMSD values suggest structural fluctuations or significant conformational changes (Figure 3).

Analyzing the RMS distribution involves examining the frequency or probability distribution of RMSD values over the simulation time. This distribution provides insights into the range of structural variability exhibited by the protein. The peaks in the RMS distribution can represent distinct conformational states or transitions among different structural motifs. Identifying and characterizing these peaks aids in understanding the dynamics and equilibrium states of the protein (Figure 3). The RMS distribution of wild-type and mutant KRas proteins was compared to assess the impact of mutations on structural stability. Differences in the distribution patterns may highlight the influence of mutations on the protein's conformational dynamics. The RMSD values for wild-type KRas ranged from 0.082 to 0.28 nm, with an average RMSD of 0.182 nm, indicative of moderate conformational fluctuations over the simulation period. Specifically, the G12C mutation exhibited an RMSD range of 0.078 to 0.29 nm, with an average RMSD of 0.177 nm. For G12D, the RMSD varied from 0.081 to 0.29 nm, with an average RMSD of 0.187 nm. G12V demonstrated RMSD values ranging from 0.081 to 0.31 nm and an average RMSD of 0.19 nm. Similarly, G13D showed an RMSD range of 0.081 to 0.27 nm, with an average RMSD of 0.172 nm. These findings highlight distinct conformational dynamics among the mutated KRas variants, with G12V and G12D exhibiting slightly higher average RMSD values compared to those of the wild type and other mutations. The observed differences in RMSD suggest potential implications for the functional dynamics of these KRas variants (Figure 4). The observed differences in RMSD among wild-type KRas and its mutated variants provide valuable insights into the impact of specific mutations on the protein's structural stability.

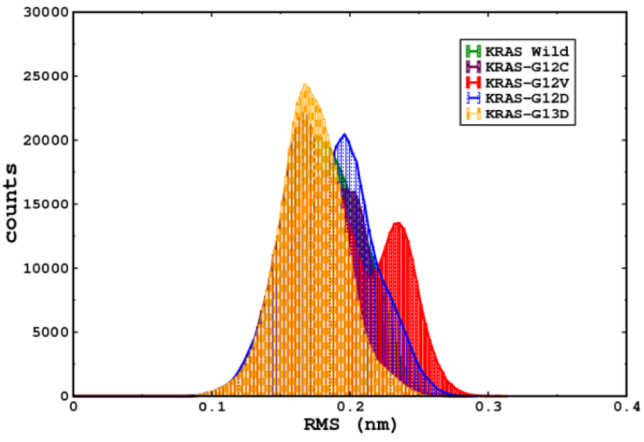

Figure 4. Root-mean-square distribution of wild-type KRas and mutant variants of KRas-G12C, G12V, G12D, and G13D.

Expanding on the biological implications of the clustering analysis results for KRas wild type and mutated variants, here, we also chose the mutated amino acids 12, 13, 51, and 118

https://doi.org/10.1021/acsomega.4c02671
ACS Omega 2024, 9, 30665−30674

amino acids that undergo mutations. In KRas wild-type, the structural stability of amino acid 12 suggests a crucial role in maintaining the overall stability of the KRas protein. It might be involved in key interactions within the protein's binding sites or activation regions. The residue 51 showed moderate flexibility and implied a certain level of adaptability. This residue may be involved in conformational changes required for signaling or interaction with downstream effectors. The residue 118 showed moderate flexibility similar to residue 51, suggesting a potential role in dynamic structural changes, possibly linked to functional transitions in KRas. The increased variability in combinations may indicate cooperative effects between these residues, potentially influencing the KRas protein function in a more intricate manner. In the G12C mutated variant, residue 12 displayed significantly low RMSD values, indicating stability. This likely plays a critical role in maintaining the structural integrity of the protein, even with the G12C mutation. The residues 51 and 118 outline the flexibility and suggest that the G12C mutation could influence the dynamic behavior of the protein, possibly impacting its interactions with other cellular components. The increased flexibility in combinations may imply synergistic effects of mutated residues on structural dynamics, which could be relevant for downstream signaling pathways. Next, in the G12D mutated variant, residue 12 showed moderate flexibility suggesting a role in structural dynamics, potentially influencing the KRas function. The low RMSD values of residue 51 indicate stability, suggesting that despite the G12D mutation this residue retains its structural integrity. The residue 118 displayed flexibility similar to residue 51 and thus maintained stability, indicating potential importance in maintaining the overall structure. The G12V that displayed moderate flexibility in residue 12 may imply a role in conformational changes required for the KRas function. The residue 51 showed lower RMSD values suggesting stability and a potentially crucial role in maintaining the structural integrity of the protein. The moderate flexibility was achieved by residue 118 may contribute to the overall structural dynamics of the protein. The higher structural flexibility in combinations indicates potential cooperative effects between mutated residues, which could influence the protein's function. Moreover, the G13D variant, residue 12 showed restrained flexibility, suggesting a role in dynamic structural changes. Residue 51 with low RMSD values indicates stability, suggesting this residue's importance in maintaining structural integrity. Residue 118 maintains stability, indicating a potential significance in the overall structure. These combination results may suggest a cooperative effect of mutated residues, potentially influencing the KRas function in a concerted manner. The overall biological implications and functional significance observed in structural variations in specific residues, especially in combinations, may impact the KRas protein function (Figures 4−7). Besides the above-detailed fluctuations among wild and mutants of Kras, we also determine the total counts (neighboring structures at cutoff mark) and average RMSD of the group of residues (r) r1-r51 and r12-r118, and they are illustrated in Figures 8, 99 and Table 1. From the understanding these changes is crucial for unraveling the molecular mechanisms underlying KRas-driven cancers. Targeting residues that exhibit maintained structural variability may provide a basis for developing novel therapeutic strategies to modulate KRas activity. The cooperative effects observed in combinations of mutated residues highlight the interconnectedness of specific amino acids in influencing the overall structural dynamics of KRas. The biological implications of the clustering analysis results underscore the importance of specific amino acid residues in KRas function and how mutations can alter the structural landscape, providing potential avenues for targeted therapeutic interventions in KRas-driven cancers.

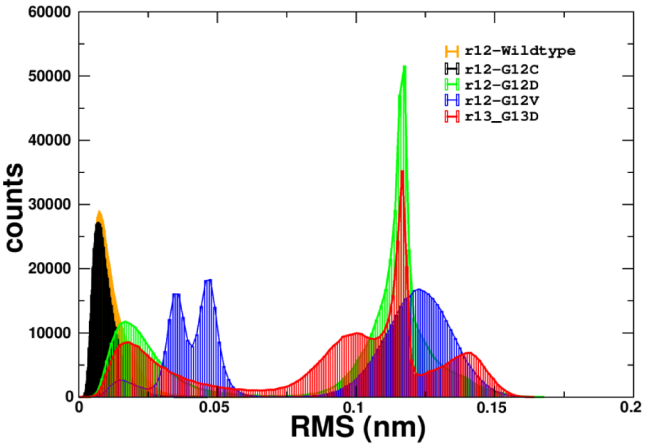

Figure 5. Average root-mean-square distribution of residues 12 and 13 of wild and mutants of the KRas.

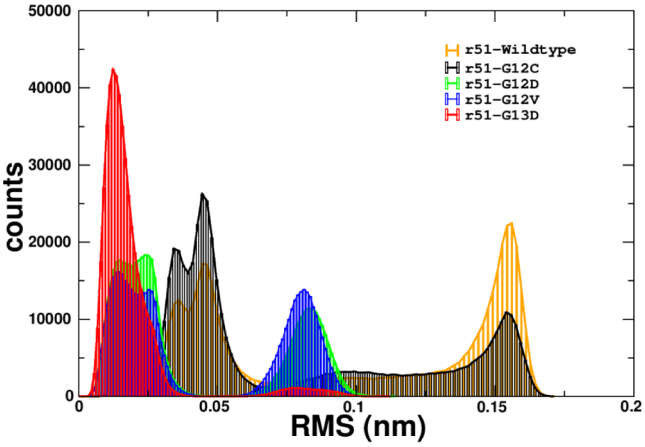

Figure 6. Average root-mean-square distribution of residue 51 of wild and mutants of the KRas.

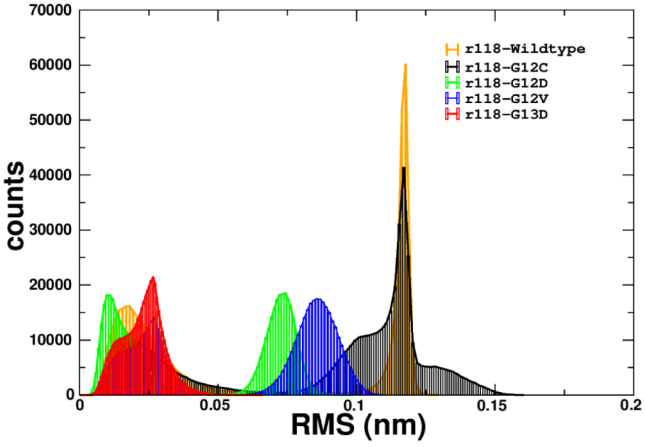

Figure 7. Average root-mean-square distribution of residue 118 wild and mutants of the KRas.

https://doi.org/10.1021/acsomega.4c02671
ACS Omega 2024, 9, 30665−30674

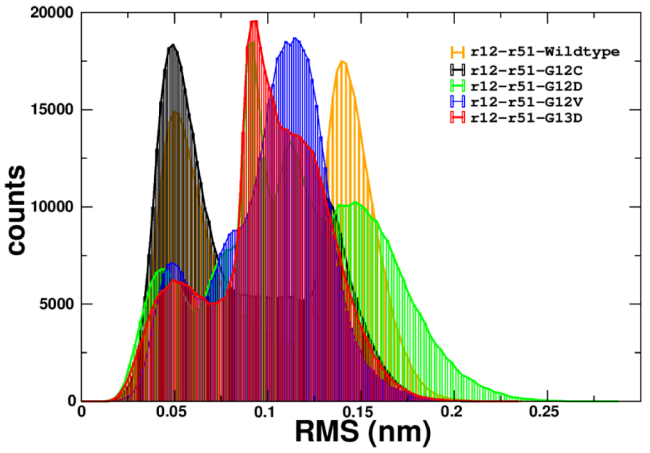

Figure 8. Average root-mean-square distribution of a group of two residues 12 and 51 of wild and mutants of the KRas.

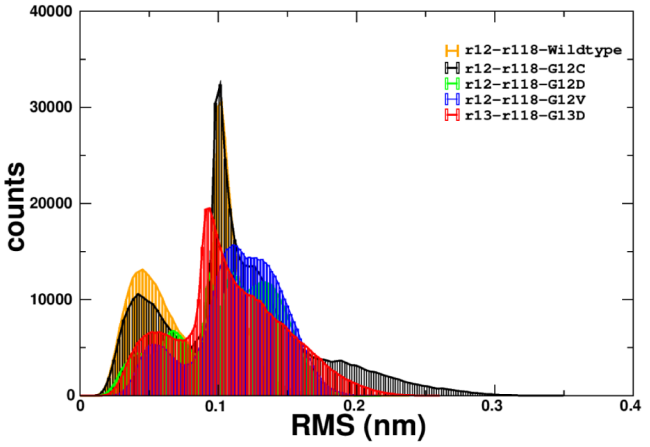

Figure 9. Average root-mean-square distribution of a group of two residues 12 and 118 of wild and mutants of the KRas.

Protein RMSD of KRas Wildtype and Mutated Variants. To differentiate the stability of the KRAS wild type and its mutated variants (KRas-G12C, G12V, G12D, G13D) based on the RMSD values, a more detailed analysis of RMSD among variants and wildtype of KRas was performes with wild type KRas: RMSD range: 0.07−0.17 nm, KRas-G12C: RMSD range: 0.07−0.15 nm, KRas-G12V: RMSD range: 0.07−0.25 nm, KRas-G12D: RMSD range: 0.07−0.17 nm, KRas-G13D: RMSD range: 0.07−0.15 nm (Figure 10). The wild type KRAS displayed a narrow RMSD range, suggesting that the wild-type structure is relatively stable during the simulation. The values are within a tight range, indicating a consistent structural behavior. Whereas, the KRas-G12C displayed a similar RMSD range to the wild type, indicating that the G12C mutation does not significantly disrupt the stability. The slightly lower upper bound may suggest a subtle increase in the stability or rigidity. Moreover, the KRas-G12V displayed a wider RMSD range, indicating a higher degree of structural variability compared to the wild type. The upper limit of 0.25 nm suggests potential conformational changes or flexibility introduced by the G12V mutation. Next, the KRas-G12D showed a similar RMSD range to the wild type, indicating that the G12D mutation does not significantly impact stability. The values falling within the wild-type range suggest structural similarity. Subsequently, the

Table 1. Average RMSD of the Amino Acids of Wild and Mutant Variants of KRas during Simulations

s. no.	KRas protein	residues	RMSD range (nm)	average RMSD (nm)
1	6mbu/ wildtype	12	0.00105459 to 0.061465	0.0116921
	6mbu/ wildtype	51	0.00651985 to 0.171463	0.0974175
	6mbu/ wildtype	118	0.00387809 to 0.129317	0.0658436
	6mbu/ wildtype	12 and 51	0.0139531 to 0.236476	0.103832
	6mbu/ wildtype	12 and 118	0.00973122 to 0.237975	0.0813918
2	6USZ/ G12C	12	0.00134581 to 0.0465652	0.00975824
	6USZ/ G12C	51	0.00591288 to 0.171179	0.0772961
	6USZ/ G12C	118	0.00399748 to 0.160367	0.0868237
	6USZ/ G12C	12 and 51	0.0142107 to 0.233619	0.100486
	6USZ/ G12C	12 and 118	0.00996376 to 0.349546	0.111868
3	7xkj/G12D	12	0.00344184 to 0.167754	0.0890734
	7xkj/G12D	51	0.00292006 to 0.113975	0.0414304
	7xkj/G12D	118	0.00292006 to 0.113975	0.0414304
	7xkj/G12D	12 and 51	0.0118171 to 0.288002	0.113453
	7xkj/G12D	12 and 118	0.0123646 to 0.217742	0.107086
4	7c40/ G12V	12	0.0052531 to 0.163563	0.0890764
	7c40/ G12V	51	0.00301193 to 0.109708	0.0449494
	7c40/ G12V	118	0.00348713 to 0.112691	0.0593161
	7c40/ G12V	12 and 51	0.0142107 to 0.233619	0.100486
	7c40/ G12V	12 and 118	0.0134572 to 0.230889	0.113934
5	6e6f/G13D	12	0.00374097 to 0.164255	0.0897901
	6e6f/G13D	51	0.00299585 to 0.112191	0.0185697
	6e6f/G13D	118	0.00294253 to 0.0662593	0.0227834
	6e6f/G13D	12 and 51	0.0120524 to 0.234378	0.0993178
	6e6f/G13D	12 and 118	0.0135755 to 0.260051	0.108382

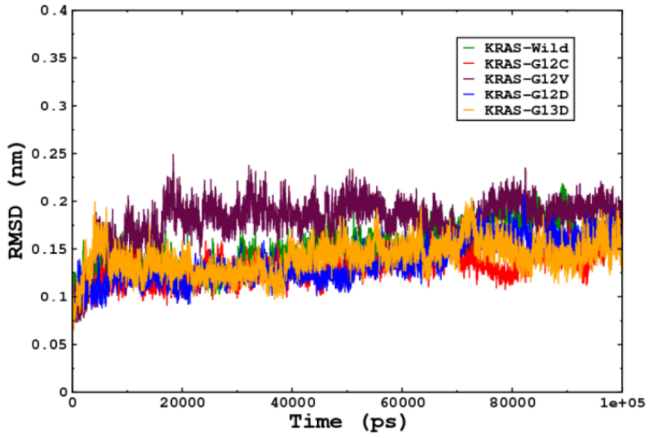

Figure 10. RMSD Cα determines the stability of the KRas wild-type and mutated variant KRas-G12C, G12V, G12D, and G13D.

https://doi.org/10.1021/acsomega.4c02671
ACS Omega 2024, 9, 30665−30674

KRas-G13D displayed that the RMSD range is within the wild-type range, indicating that the G13D mutation does not dramatically affect stability. The upper bound of 0.2 nm suggests a moderate level of structural variability. The overall comparison showed that G12C and G12D variants tend to have similar stability to that of the wild type. The minor variations in the upper or lower RMSD bounds may indicate subtle differences in the local structural dynamics. The G12V variant displays a wider RMSD range, suggesting a higher structural variability. That usually indicates potential conformational changes or increased flexibility introduced by the G12V mutation. Furthermore, the G13D variant exhibits stability comparable to that of the wild type. The moderate upper bound suggests a moderate level of structural variability. This detailed analysis allows for a nuanced understanding of the stability differences among the KRas variants, providing valuable insights into their structural behavior during simulations.

Flexibility of Each Amino Acid in KRAS Wildtype and Mutated Variants. Root mean square fluctuation (RMSF) is a measure of the flexibility or mobility of individual atoms or groups of atoms in a molecular system, often calculated over a trajectory obtained from molecular dynamics simulations. It provides insight into the dynamic behavior of specific regions within a protein. The overall RMSF values indicate relatively stable behavior during the simulation. Specific residues (28−42, 57−67) and RMSF values in the range of 0.05−0.4 nm suggest some level of flexibility or variability in these regions (Figure 11). While the protein as a whole remains stable,

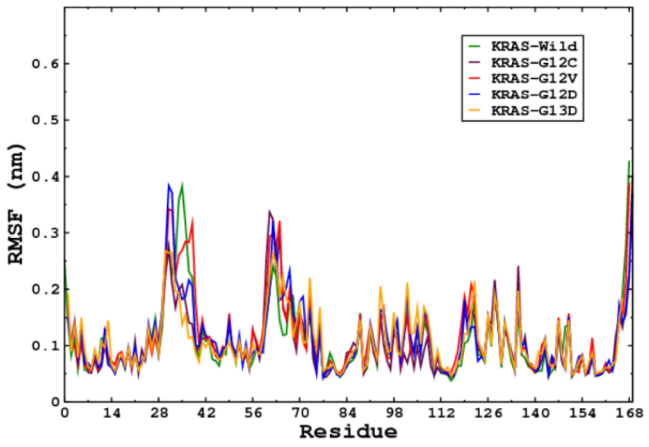

Figure 11. Root-mean-square fluctuation (RMSF) of KRAS wild-type and mutated variant KRAS-G12C, G12V, G12D, and G13D.

certain regions (28−42, 57−67) display fluctuations, which might be functionally relevant or reflect local flexibility; the rest of the amino acids showed flexibility of 0.05−0.2 nm. The KRAS-G12C showed that the overall RMSF profile is similar to that of the wild type. The G12C mutation does not seem to introduce significant changes in the flexibility pattern compared with the wild type. The residues 28−42 and 57−67 maintain similar fluctuation levels. Next, the KRas-G12V showed that the RMSF profile is comparable to that of the wild type. The G12V mutation does not induce drastic changes in the flexibility. The residues 28−42 and 57−67 continue to show similar fluctuation levels to the wild type. Moreover, the RMSF profile showed by the KRAS-G12D aligns with the wild type. The G12D mutation maintains flexibility patterns similar to those of the wild type. Residues 28−42 and 57−67 exhibit comparable fluctuation levels. The KRas-G13D RMSF profile closely resembles that of the wild type. The G13D mutation does not lead to significant alterations in the flexibility. Residues 28−42 and 57−67 show similar fluctuation patterns. The mutants (G12C, G12V, G12D, and G13D) do not exhibit substantial changes in overall flexibility compared to the wild type. Residues 28−42 and 57−67 in all variants display similar RMSF patterns to the wild type, suggesting that the mutations do not induce major alterations in the flexibility of these specific regions. While RMSF provides information about flexibility, functional implications depend on the specific role of the residues in these regions. RMSF results are combined with RMSF analysis for a comprehensive understanding of both overall stability and local flexibility. This detailed analysis of RMSF values indicates that, while there are fluctuations in specific regions (28−42, 57−67), these fluctuations are consistent across the wild type and mutated variants. The mutations (G12C, G12V, G12D, and G13D) do not seem to introduce significant changes in the flexibility patterns of these specific regions compared to the wild type. The fluctuations that occurred in were found approximately similar to the data reported by Maitra et al.[27]

Radius of Gyration (RoG) of KRas Wildtype and Mutated Variants. The RoG values indicate a relatively compact structure for the wild type. The narrow range suggests stable behavior during the simulation. The wild-type KRas maintains a consistent and compact overall structure. The KRas-G12C showed RoG values lesser than wild type, suggesting that the G12C mutation showed significant alteration in the overall size or compactness. The G12C mutation appears to have a minimal effect on the overall structure in terms of size and compactness. The KRas-G12V displayed RoG values comparable to the wild type suggesting that the G12V mutation does not induce major changes in compactness. Moreover, the G12V mutation appears to have a minimal impact on the overall structure in terms of size and compactness. The KRas-G12D showed RoG values lesser than wild type indicating that the G12D mutation does not lead to significant alterations in overall size or compactness. The G12D mutation appears to have a minimal impact on the overall structure in terms of size and compactness. The G13 V mutation appears to have a minimal impact on the overall structure in terms of size and compactness. All mutants (G12C, G12V, G12D, G13D) exhibit RoG values lower than that of the wild type (Figure 12). The mutations may significantly alter the overall size or compactness of the KRas protein. The dynamic changes in a system were calculated in the form of the RoG, which provides information on overall size; it does not capture dynamic changes in specific regions. The combined RoG results from RMSD and RMSF analyses provide a comprehensive understanding of both overall stability and local flexibility.

Solvent Accessible Surface Area (SASA) of KRas Wildtype and Mutated Variants. The SASA is a measure of the surface area of a protein or macromolecules that is accessible to solvent molecules. It provides information about the degree of exposure of a molecule to its environment, which can be indicative of its solvation and interaction properties. In the context of proteins, SASA is often used to assess the accessibility of amino acid residues to solvent molecules. The wild-type KRas showed higher SASA values, suggesting that the wild-type KRas has a relatively less solvent-exposed surface.

https://doi.org/10.1021/acsomega.4c02671
ACS Omega 2024, 9, 30665−30674

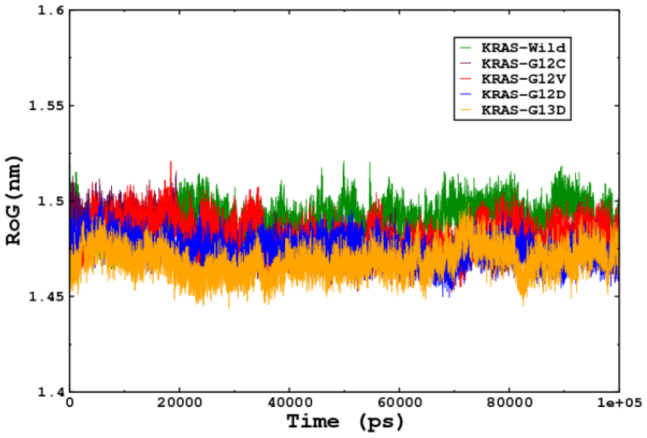

Figure 12. Compactness of the KRas wild-type and mutant variants KRAS-G12C, G12V, G12D, and G13D.

The wild-type KRAS tends to have a surface that is less accessible to solvent molecules, possibly indicating a more open conformation. The KRas-G12C showed SASA values approximately similar to the wild type, suggesting that the G12C mutation leads to a compactness. The G12C mutation appears to decrease the accessibility of the protein surface to solvent molecules, potentially indicating dynamic conformation. The SASA of KRas-G12V displayed similarity to G12C, and the G12V mutation results in higher SASA values compared to the wild type. The G12V mutation decreases the accessibility of the protein surface, suggesting a potential increase in compactness. The KRas-G12D almost showed similarity to G12C and G12V, and the G12D mutation leads to lower SASA values compared to the wild type. The G12D mutation decreases the solvent accessibility, indicating a potential shift toward a more open or dynamic conformation. The KRas-G13D showed similarity to other mutants; G13D exhibits lower SASA values compared to the wild type. The G13D mutation decreases the accessibility of the protein surface, suggesting a potential increase in lesser flexibility than other variants and wildtype (Figure 13). The SASA analysis suggests that the mutations (G12C, G12V, G12D, and G13D) in KRas lead to decreased solvent accessibility compared to the wild type, indicating dynamic structure for the mutant variants.

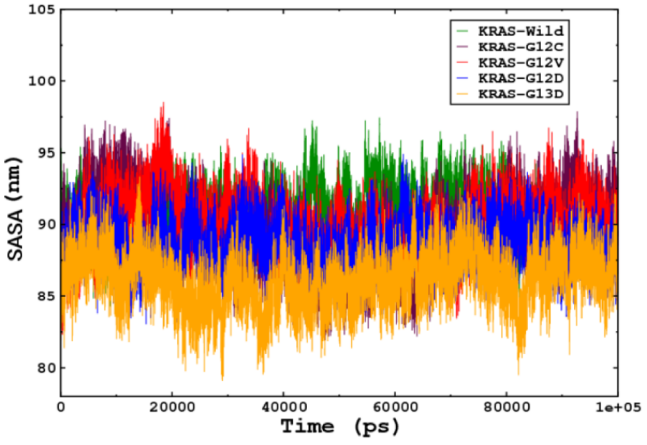

Figure 13. Solvent accessible surface area (SASA) for each complex was determined by wild-type KRas and the mutated variants of KRas-G12C, G12V, G12D, and G13D.

Principal Components of KRas Wildtype and Mutated Variants. This principal component analysis (PCA) was employed to unravel the conformational dynamics of wild-type KRas and its G12C, G12D, G12V, and G13D mutated variants. Molecular dynamics simulations conducted using GROMACS software provide detailed insights into the principal components, offering a nuanced understanding of the protein's structural variability. The wild-type KRas, PC1 spans from −1.75 to 1.4, indicating significant structural variance along this principal component. PC2 ranges from −1 to 1, showing diverse conformations captured during the simulation. Next, the G12C mutated variant, PC1 exhibits a broader range from −2 to 1.75, reflecting increased conformational variability compared with the wild type. PC2 ranges from −1.4 to 1.2, suggesting distinct structural arrangements. Moreover, the G12D mutated variant PC1 varies between −1.6 and 1.1, indicating unique conformational transitions. PC2 ranges from −1 to 1, capturing additional structural nuances. Furthermore, the G12V mutated variant, PC1 extends from −1.5 to 0.6, showing altered dynamics compared to the wild type. PC2 ranges from −1.2 to 1.3, revealing diverse conformations. Finally, the G13D mutated variant PC1 spans from −0.4 to 1.1, suggesting a distinctive conformational landscape. PC2 ranges from −0.8 to 1.1, indicating specific structural variations (Figure 14). These PCA results highlight

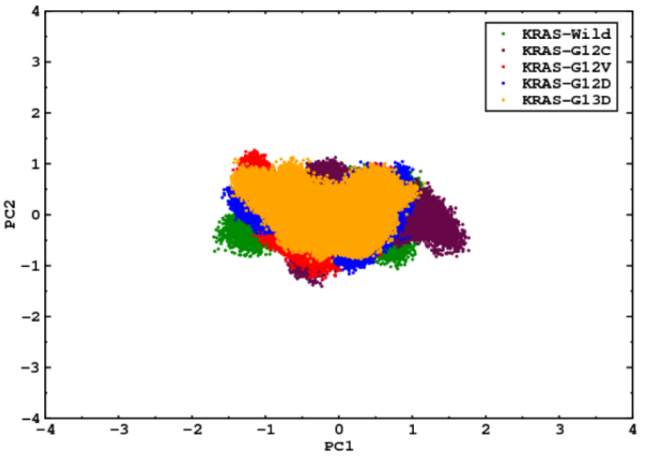

Figure 14. PCA KRas wildtype and mutated variants.

pronounced differences in the conformational dynamics among wild-type KRas and its mutated variants. The broader ranges and unique patterns observed in the mutated variants suggest that specific mutations influence the protein's structural flexibility and may have functional implications. The PCA results shed light on the conformational dynamics of KRas and its mutated variants. The observed variations along PC1 and PC2 provide a basis for understanding the impact of mutations on the protein's structural plasticity, offering insights that could inform targeted drug design strategies.

Free Energy Surfaces of KRas Wildtype and Mutated Variants. This Gibbs energy landscape analysis was employed to explore the conformational stability of wild-type KRas and its G12C, G12D, G12V, and G13D mutated variants. The free energy landscape (FEL) calculations provide a comprehensive view of the thermodynamic stability of these proteins. The Gibbs energy landscape analysis for wild-type KRas yields FEL values ranging from 0 to 18.7 kJ/mol, portraying the energetic stability of various conformations sampled during the

https://doi.org/10.1021/acsomega.4c02671
ACS Omega 2024, 9, 30665−30674

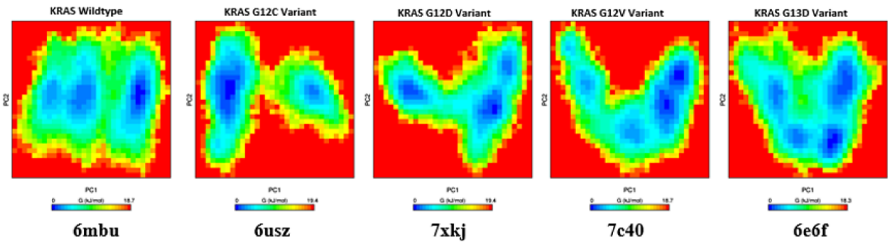

Figure 15. Gibbs energy landscape of KRas wild-type and mutated variants.

simulation. The FEL values for the G12C mutated variant span from 0 to 19.4 kJ/mol, suggesting alterations in the conformational stability compared with that of the wild type. Similarly, for the G12D mutated variant, the FEL values range from 0 to 19.4 kJ/mol, indicating shifts in the thermodynamic landscape in relation to the wild type. The Gibbs energy landscape analysis for the G12V mutated variant shows FEL values from 0 to 19.4 kJ/mol, highlighting potential changes in the conformational stability. For the G13D mutated variant, the FEL values range from 0 to 18.7 kJ/mol, providing insights into the energetic landscape of this mutated form similar to wildtype (Figure 15). These results suggest distinct variations in the conformational stability of the KRas protein and its mutated variants, indicating the influence of specific mutations on the thermodynamic characteristics. The observed differences in FEL values among wild-type KRas and its mutated variants reveal variations in conformational stability. The alterations in the Gibbs energy landscape may correlate with functional changes in the protein structure, providing valuable insights into understanding the impact of mutations on KRas behavior. These findings contribute to a deeper understanding of the thermodynamic aspects of KRas conformational dynamics and may have implications for drug design and targeted therapies.

CONCLUSION

In conclusion, this study employed a comprehensive approach to investigate the structural dynamics of wild-type KRas and its mutated variants (G12C, G12D, G12V, and G13D) through sequence alignment, molecular dynamics simulations, clustering analysis, and various structural analyses. The selected mutated variants were of particular interest due to their relevance to oncogenic transformation. The research utilized X-ray crystallographic structures obtained from the Protein Data Bank (PDB) and performed sequence alignment using Clustal Omega, followed by molecular dynamics simulations. The sequence alignment revealed distinct mutations at key positions, such as G12 and G13, within the GTP-binding domain of KRas. Molecular dynamics simulations provided insights into the conformational dynamics and stability of the proteins, revealing variations in the root-mean-square deviation (RMSD) among wild-type and mutated variants. Clustering analysis identified higher conformational changes in the second α-helix of mutated variants. The study further analyzed the root-mean-square fluctuation (RMSF), radius of gyration (RoG), solvent accessible surface area (SASA), principal components, and free energy surfaces, providing a comprehensive understanding of the structural variations and stability of KRas and its mutants. The results highlighted that G12V and G12D mutants exhibited slightly higher average RMSD values, suggesting potential implications for their functional dynamics compared to those of other mutants and the wild type. Clustering analysis pinpointed residues crucial for stability and flexibility, emphasizing the interconnectedness of specific amino acids in influencing the overall structural dynamics of KRas. The mutants displayed distinct RMSF profiles, indicating conserved flexibility in specific regions across all variants. Furthermore, RoG analysis suggested that mutations led to alterations in the overall size of KRas, with mutants generally exhibiting RoG values lower than those of the wild type. SASA analysis indicated decreased solvent accessibility in mutants compared with the wild type, suggesting a potential shift toward a more dynamic conformation. Principal component analysis (PCA) and free energy landscape (FEL) analysis revealed pronounced differences in conformational dynamics and thermodynamic stability among the wild-type and mutated variants. Overall, the detailed analyses provided valuable insights into the structural dynamics and stability of KRas and its mutated variants, shedding light on the molecular mechanisms underlying KRas-driven cancers. These findings contribute to ongoing efforts in designing targeted therapeutic strategies for KRas-mutated cancers, offering a basis for the development of novel treatments aimed at modulating KRas activity.

AUTHOR INFORMATION

Corresponding Authors

Binata Nayak − *School of Life Sciences, Sambalpur University, Burla, Odisha 768019, India*; Email: binatanayak@suniv.ac.in

Vinoth Kumarasamy − *Department of Parasitology and Medical Entomology, Faculty of Medicine, Universiti Kebangsaan Malaysia, Kuala Lumpur 56000, Malaysia*; orcid.org/0000-0002-8895-1796; Email: vinoth@ukm.edu.my

Bikram Dhara − *Center for Global Health Research, Saveetha Medical College and Hospital, Saveetha Institute of Medical and Technical Sciences, Chennai, Tamil Nadu 602105, India; Department of Health Sciences, Novel Global Community Educational Foundation, Hebersham, New South Wales 2770, Australia*; orcid.org/0000-0002-5433-1994; Email: bikramdhara@sxccal.edu

Authors

Showkat Ahmad Mir − *School of Life Sciences, Sambalpur University, Burla, Odisha 768019, India*; orcid.org/0000-0002-3668-2184

Nada H Aljarba − *Department of Biology, College of Science, Princess Nourah bint Abdulrahman University, Riyadh 11671, Saudi Arabia*

Vetriselvan Subramaniyan − *Jeffrey Cheah School of Medicine and Health Sciences, Monash University Malaysia, Bandar Sunway, Selangor Darul Ehsan 47500, Malaysia*; orcid.org/0000-0002-9629-9494

https://doi.org/10.1021/acsomega.4c02671
ACS Omega 2024, 9, 30665−30674

Complete contact information is available at:
https://pubs.acs.org/10.1021/acsomega.4c02671

Author Contributions

Conceptualization, Study Design, Writing Original Draft: Showkat Ahmad Mir, Binata Nayak, Nada H Aljarba, Bikram Dhara; Review and Editing: Vinoth Kumarasamy, Vetriselvan Subramaniyan.

Notes

The authors declare no competing financial interest.

■ ACKNOWLEDGMENTS

This work was funded by the Princess Nourah bint Abdulrahman University Researchers Supporting Project (no. PNURSP2024R62), Princess Nourah bint Abdulrahman University, Riyadh, Saudi Arabia.

■ REFERENCES

(1) Huang, L.; Guo, Z.; Wang, F.; Fu, L. KRAS mutation: from undruggable to druggable in cancer. *Signal Transduct. Target. Ther.* **2021**, *6* (1), 386.
(2) Hanahan, D.; Weinberg, R. A. Hallmarks of Cancer: The Next Generation. *Cell* **2011**, *144* (5), 646−674.
(3) Prior, I. A.; Lewis, P. D.; Mattos, C. A Comprehensive Survey of Ras Mutations in Cancer. *Cancer Res.* **2012**, *72* (10), 2457−2467.
(4) Sever, R.; Brugge, J. S. Signal Transduction in Cancer. *Cold Spring Harb. Perspect. Med.* **2015**, *5* (4), a006098−a006098.
(5) Stephen, A. G.; Esposito, D.; Bagni, R. K.; McCormick, F. Dragging Ras Back in the Ring. *Cancer Cell* **2014**, *25* (3), 272−281.
(6) Ostrem, J. M. L.; Shokat, K. M. Direct small-molecule inhibitors of KRAS: from structural insights to mechanism-based design. *Nat. Rev. Drug Discovery* **2016**, *15* (11), 771−785.
(7) Hunter, J. C.; Manandhar, A.; Carrasco, M. A.; Gurbani, D.; Gondi, S.; Westover, K. D. Biochemical and Structural Analysis of Common Cancer-Associated KRAS Mutations. *Mol. Cancer Res.* **2015**, *13* (9), 1325−1335.
(8) Pettersen, E. F.; Goddard, T. D.; Huang, C. C.; Couch, G. S.; Greenblatt, D. M.; Meng, E. C.; Ferrin, T. E. UCSF Chimera—A visualization system for exploratory research and analysis. *J. Comput. Chem.* **2004**, *25* (13), 1605−1612.
(9) Han, C. W.; Jeong, M. S.; Ha, S. C.; Jang, S. B. A H-REV107 Peptide Inhibits Tumor Growth and Interacts Directly with Oncogenic KRAS Mutants. *Cancers* **2020**, *12* (6), 1412.
(10) Akash, S.; Bayıl, I.; Mahmood, S.; Mukerjee, N.; Mili, T. A.; Dhama, K.; Rahman, M. A.; Maitra, S.; Mohany, M.; Al-Rejaie, S. S.; Ali, N. Mechanistic inhibition of gastric cancer-associated bacteria Helicobacter pylori by selected phytocompounds: A new cutting-edge computational approach. *Heliyon* **2023**, *9* (10), No. e20670.
(11) Humphrey, W.; Dalke, A.; Schulten, K. VMD: Visual molecular dynamics. *J. Mol. Graph.* **1996**, *14* (1), 33−38.
(12) Chakrobarty, S.; Garai, S.; Ghosh, A.; Mukerjee, N.; Das, D. Bioactive plantaricins as potent anti-cancer drug candidates: double docking, molecular dynamics simulation and in vitro cytotoxicity analysis. *J. Biomol. Struct. Dyn.* **2023**, *41* (23), 13605−13615.
(13) Sievers, F.; Wilm, A.; Dineen, D.; Gibson, T. J.; Karplus, K.; Li, W.; Lopez, R.; McWilliam, H.; Remmert, M.; Söding, J.; Thompson, J. D. Fast, scalable generation of high-quality protein multiple sequence alignments using Clustal Omega*Mol. Syst. Biol.***2011**71
(14) McWilliam, H.; Li, W.; Uludag, M.; Squizzato, S.; Park, Y. M.; Buso, N.; Cowley, A. P.; Lopez, R. Analysis Tool Web Services from the EMBL-EBI. *Nucleic Acids Res.* **2013**, *41* (W1), W597−W600.
(15) Berman, H. M. The Protein Data Bank. *Nucleic Acids Res.* **2000**, *28* (1), 235−242.
(16) Berendsen, H. J. C.; van der Spoel, D.; van Drunen, R. GROMACS: A message-passing parallel molecular dynamics implementation. *Comput. Phys. Commun.* **1995**, *91* (1−3), 43−56.
(17) Meher, R. K.; Mir, S. A.; Singh, K.; Mukerjee, N.; Nayak, B.; Kumer, A.; Zughaibi, T. A.; Khan, M. S.; Tabrez, S. Decoding dynamic interactions between EGFR-TKD and DAC through computational and experimental approaches: A novel breakthrough in lung melanoma treatment. *J. Cell. Mol. Med.* **2024**, *28* (9), No. e18263.
(18) Maier, J. A.; Martinez, C.; Kasavajhala, K.; Wickstrom, L.; Hauser, K. E.; Simmerling, C. ff14SB: Improving the Accuracy of Protein Side Chain and Backbone Parameters from ff99SB. *J. Chem. Theory Comput.* **2015**, *11* (8), 3696−3713.
(19) Mir, S. A.; Nayak, B. In Silico Analysis of Binding Stability of Quercetin with CmpA and In Vitro Growth Inhibition Study of Cyanobacterial Species Using Azadirachta indica Extracts. *Chem. Afr.* **2022**, *5* (3), 691−701.
(20) Mir, S. A.; Dash, G. C.; Meher, R. K.; Mohanta, P. P.; Chopdar, K. S.; Mohapatra, P. K.; Baitharu, I.; Behera, A. K.; Raval, M. K.; Nayak, B. In Silico and In Vitro Evaluations of Fluorophoric Thiazolo-[2,3-b]quinazolinones as Anti-cancer Agents Targeting EGFR-TKD. *Appl. Biochem. Biotechnol.* **2022**, *194* (10), 4292−4318.
(21) Ahmad Mir, S.; Meher, R. K.; Baitharu, I.; Nayak, B. Molecular dynamic simulation, free binding energy calculation of Thiazolo-[2,3-b]quinazolinone derivatives against EGFR-TKD and their anticancer activity. *Results Chem.* **2022**, *4*, 100418.
(22) Mir, S. A.; Muhammad, A.; Padhiary, A.; Ekka, N. J.; Baitharu, I.; Naik, P. K.; Nayak, B. Identification of potent EGFR-TKD inhibitors from NPACT database through combined computational approaches. *J. Biomol. Struct. Dyn.* **2023**, *41* (21), 12063−12076.
(23) Akash, S.; Aovi, F. I.; Azad, M. A.; Kumer, A.; Chakma, U.; Islam, M. R.; Mukerjee, N.; Rahman, M. M.; Bayıl, I.; Rashid, S.; et al. A drug design strategy based on molecular docking and molecular dynamics simulations applied to development of inhibitor against triple-negative breast cancer by Scutellarein derivatives. *PLoS One* **2023**, *18* (10), No. e0283271.
(24) Vetter, I. R.; Wittinghofer, A. The Guanine Nucleotide-Binding Switch in Three Dimensions. *Science* **2001**, *294* (5545), 1299−1304.
(25) Vatansever, S.; Erman, B.; Gümüş, Z. H. Oncogenic G12D mutation alters local conformations and dynamics of K-Ras. *Sci. Rep.* **2019**, *9* (1), 11730.
(26) Vatansever, S.; Erman, B.; Gümüş, Z. H. Comparative effects of oncogenic mutations G12C, G12V, G13D, and Q61H on local conformations and dynamics of K-Ras. *Comput. Struct. Biotechnol. J.* **2020**, *18*, 1000−1011.
(27) Maitra, S.; Mukerjee, N.; Alharbi, H. M.; Ghosh, A.; Alexiou, A.; Thorat, N. D. Targeted therapies for HPV-associated cervical cancer: Harnessing the potential of exosome-based chipsets in combating leukemia and HPV-mediated cervical cancer. *J. Med. Virol.* **2024**, *96* (4), No. e29596.
(28) Pantsar, T.; Rissanen, S.; Dauch, D.; Laitinen, T.; Vattulainen, I.; Poso, A.; Nussinov, R. Assessment of mutation probabilities of KRAS G12 missense mutants and their long-timescale dynamics by atomistic molecular simulations and Markov state modeling. *PloS Comput. Biol.* **2018**, *14* (9), No. e1006458.
(29) Saha, P.; Hegde, M.; Chakraborty, K.; Singha, A.; Mukerjee, N.; Ghosh, D.; Kunnumakkara, A. B.; Khan, M. S.; Ahmad, M. I.; Ghosh, A.; et al. Targeted inhibition of colorectal cancer proliferation: The dual-modulatory role of 2, 4-DTBP on anti-apoptotic Bcl-2 and Survivin proteins. *J. Cell. Mol. Med.* **2024**, *28* (7), No. e18150.
(30) Ahamed, A.; Samanta, A.; Alam, S. S. M.; Mir, S. A.; Jamil, Z.; Ali, S.; Hoque, M. Nonsynonymous mutations in VEGF receptor binding domain alter the efficacy of bevacizumab treatment. *J. Cell. Biochem.* **2024**, *125* (2), No. e30515.